Enhanced Photoluminescence and Solar Cell Performance *via* Lewis Base Passivation of Organic–Inorganic Lead Halide Perovskites

Nakita K. Noel,[†] Antonio Abate,[†] Samuel D. Stranks,[†] Elizabeth S. Parrott,[†] Victor M. Burlakov,[‡] Alain Goriely,[‡] and Henry J. Snaith*[,†]

[†]Clarendon Laboratory, Department of Physics, University of Oxford, Parks Road, Oxford OX1 3PU, United Kingdom and [‡]Mathematical Institute, University of Oxford, Andrew Wiles Building, Radcliffe Observatory Quarter, Woodstock Road, Oxford OX2 6GG, United Kingdom

ABSTRACT Organic–inorganic metal halide perovskites have recently emerged as a top contender to be used as an absorber material in highly efficient, low-cost photovoltaic devices. Solution-processed semiconductors tend to have a high density of defect states and exhibit a large degree of electronic disorder. Perovskites appear to go against this trend, and despite relatively little knowledge of the impact of electronic defects, certified solar-to-electrical power conversion efficiencies of up to 17.9% have been achieved. Here, through treatment of the crystal surfaces with the Lewis bases thiophene and pyridine, we demonstrate significantly reduced nonradiative electron–hole recombination within the $CH_3NH_3PbI_{3-x}Cl_x$ perovskite, achieving photoluminescence lifetimes which are enhanced by nearly an order of magnitude, up to 2 μs. We propose that this is due to the electronic passivation of under-coordinated Pb atoms within the crystal. Through this method of Lewis base passivation, we achieve power conversion efficiencies for solution-processed planar heterojunction solar cells enhanced from 13% for the untreated solar cells to 15.3% and 16.5% for the thiophene and pyridine-treated solar cells, respectively.

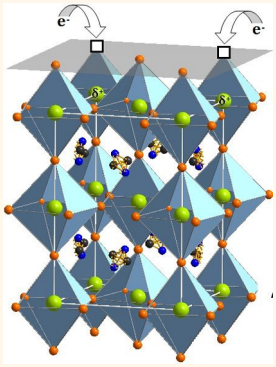

KEYWORDS: organic–inorganic perovskite · coordinate bonding · perovskite solar cells · surface passivation · under-coordinated atoms · photoluminescence · defect sites

The term perovskite encompasses all materials which have the same crystal structure as calcium titanate ($CaTiO_3$) and the chemical formula ABX_3. In the case of the organic–inorganic metal halide perovskites, the A site is occupied by an organic cation and the B site by a divalent metal ion, while the X site is occupied by a halide ion. With respect to photovoltaic energy conversion, the most well-known members of this family are the methylammonium trihalogen plumbates ($CH_3NH_3PbX_3$), where X can be either a single halogen or a mixture of halogens. $CH_3NH_3PbI_3$ and $CH_3NH_3PbBr_3$ were first used by Miyasaka in 2009[1] as sensitizers in liquid electrolyte solar cells, achieving power conversion efficiencies of 3.5%, a method which was then later optimized by Im *et al.* achieving an efficiency of 6.5%.[2] However, the instability of this material in a polar, redox electrolyte catalyzed the move to solid-state hole-transporting materials (HTMs) such as 2,2′,7,7′-tetrakis-(*N*,*N*-*p*-dimethoxyphenylamino)-9-9′-spirobifluorene (spiro-OMeTAD).[3,4] Since 2012, research into perovskite solar cells has "erupted", and the devices have evolved from a perovskite-sensitized, nanostructured configuration utilizing mesoporous TiO_2[3−6] to the meso-superstructured solar cell configuration, which makes use of an insulating material as a mesoporous scaffold,[4,7,8] to a simple planar heterojunction,[9−12] all of which have reached reported efficiencies of over 15%. This material has also been shown to operate well in "inverted" cell architectures, where the polarity of the electrodes is reversed, achieving power conversion efficiencies of up to 15%.[6,13−16]

The perovskite crystal, like most other ionic materials (*e.g.*, GaAs),[17] contains under-coordinated ions at its crystal surfaces and also at the grain boundaries between individual crystals. There have been some

* Address correspondence to h.snaith1@physics.ox.ac.uk.

Received for review July 4, 2014 and accepted August 29, 2014.

Published online August 29, 2014
10.1021/nn5036476

recent theoretical studies on the defect chemistry in these hybrid compounds. Although defect sites can occur, for instance halide vacancies, the energy of these sites should be very close to the conduction band edge,[18,19] potentially justifying the already remarkable performance of perovskite solar cells. However, there remain many imperfect qualities of the perovskite semiconductors, such as relatively high nonradiative recombination rates (inferred from low PL efficiency) under both low excitation densities and when the perovskite material is processed within a mesoporous scaffold.[20,21] Hence, considerable scope remains for further enhancement to attain the maximum performance levels.[18,22] Recently, we have demonstrated that excess iodine ions on the surface of $CH_3NH_3PbI_{3-x}Cl_x$ crystals can be passivated using the organic molecule iodopentafluorobenzene (IPFB).[23] An excess of charge building up at the crystal surface, as a result of these under-coordinated ions, has an undesirable effect on the performance of solar cells since it appears to result in an accumulation of photogenerated positive carriers within the hole-transporter phase at the heterojunction. This results in an increased level of recombination at this interface. We have shown that passivating films of $CH_3NH_3PbI_{3-x}Cl_x$ with IPFB before the deposition of the HTM negates this effect, resulting in decreased recombination in these devices as compared to the unpassivated control devices.[23] However, we note that this type of passivation appears to have a negligible influence on the perovskite material when not incorporated into the solar cell heterojunction.

Here, we employ the organic Lewis bases thiophene and pyridine with the intention of passivating the crystal surfaces of the mixed-halide, lead-based perovskite, $CH_3NH_3PbI_{3-x}Cl_x$. In order to investigate the feasibility and impact of these Lewis base treatments, we perform a spectroscopic, theoretical, and device-based investigation. We observe significantly inhibited nonradiative decay within the treated perovskite films, especially under low levels of photoexcitation. Planar heterojunction devices made utilizing the passivating agents resulted in power conversion efficiencies of 15.3 and 16.5% for thiophene- and pyridine-treated devices, respectively, with average power conversion efficiencies increasing from 12 $\pm$ 1.5% to 14 $\pm$ 1.5% and 15.5 $\pm$ 1% for the control and the thiophene- and pyridine-passivated devices, respectively.

When $CH_3NH_3PbI_{3-x}Cl_x$ films are annealed in air, we expect oxygen and water to absorb onto the surface of the crystals, resulting in the formation of lead oxide and hydroxide species,[24,25] thus in part negating the necessity for further passivation of under-coordinated Pb ions. However, it is unlikely that all, or the majority, of these states would be passivated during the relatively short annealing process, potentially creating the necessity for further chemical passivation. We propose that the observed decrease in nonradiative decay occurs due to passivation of under-coordinated Pb atoms in the perovskite crystal *via* coordinate bonding between the sulfur atom in thiophene or nitrogen atom in pyridine with under-coordinated lead ions in the perovskite. While the exact mechanism of passivation is subject to further investigation, we believe that Lewis base treatment of these perovskite films will be able to provide a more controlled and efficient method of passivating defect states, especially when the material is processed in inert atmosphere.

RESULTS AND DISCUSSION

In order to probe the fundamental impact of coating the perovskite films with thiophene or pyridine, we studied the photoluminescence properties of the films with and without these treatments. All materials which absorb light must also re-emit that light, following the Einstein rules for absorption and emission.[26] However, all other electron–hole recombination processes are non-essential and represent further losses in a solar cell material. Hence, by studying the photoluminescence of the photoactive layer of the solar cell, which is processed or treated in different ways, we can assess the impact of such steps upon the nonradiative decay channels. In Figure 1b, we show the photoluminescence quantum efficiency (PLQE) of $CH_3NH_3PbI_{3-x}Cl_x$ films with and without the thiophene and pyridine treatments. For the control films (without treatments), the PLQE rises with increasing fluence, which we have previously attributed to a filling of trap states, where the PLQE only reaches a peak value when the trap states responsible for nonradiative recombination are predominantly filled.[20,27] Notably, the PLQE is higher at all excitation intensities for both treated films and is much higher at low excitation intensities for the pyridine-treated films.

Consistent with the enhanced PLQE, we observe close to an order of magnitude increase in the PL lifetime (Figure 1a) of the perovskite films, from 340.7 $\pm$ 1.1 to 2016.5 $\pm$ 5.3 ns when the surface is treated with pyridine and to 2234.2 $\pm$ 4.2 ns when treated with thiophene, where the lifetimes are determined from monomolecular tail fits to the PL decays. If we assume the previously calculated diffusion coefficient for electrons and holes ($\sim$0.05 $cm^2\ s^{-1}$)[28] the enhanced lifetime of $\sim$2000 ns corresponds to a charge diffusion length of 3 microns. The increased PLQE and PL lifetimes indicate an overall reduction in the rate of nonradiative recombination within the material and are evidence that some of the pathways to nonradiative recombination, such as trap-mediated recombination, have been substantially reduced. If we attribute this rise in PLQE with excitation power to the filling of traps, which would otherwise facilitate nonradiative recombination, the trend we observe here is indicative of both pyridine and thiophene passivating trap states

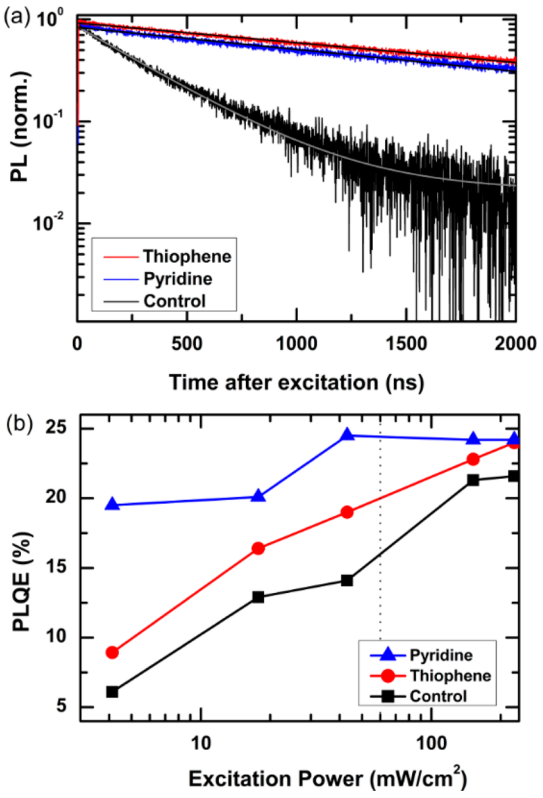

Figure 1. Photoluminescence characteristics of as-prepared (control) and thiophene- and pyridine-passivated $CH_3NH_3PbI_{3-x}Cl_x$ films. (a) Time-resolved photoluminescence of thiophene- and pyridine-passivated perovskite films as compared to as-prepared films following a 507 nm pulsed excitation (200 kHz, 30 nJ/cm^2/pulse). PL decays were acquired at the peak emission wavelength (780 nm) after 10 min stabilization under pulsed light. Solid lines are fits to the data using monoexponential tail fits. (b) Photoluminescence quantum efficiency of as-prepared films and films treated with thiophene and pyridine as a function of 532 CW laser excitation intensity. The dashed line shows the equivalent intensity to 1 sun illumination, approximately corresponding to the pulse excitation density in (a). All films were coated with PMMA to protect the perovskite from atmospheric degradation.

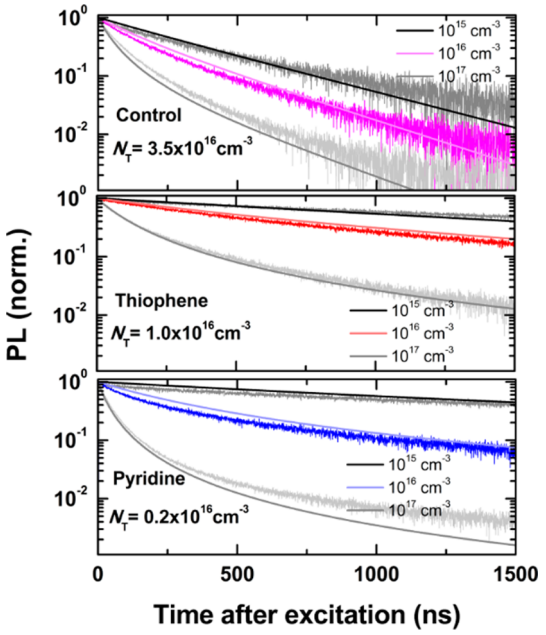

Figure 2. Photoluminescence characteristics of bare and thiophene- or pyridine-passivated films. Time-resolved PL measurements of control, thiophene, and pyridine samples with 507 nm pulsed (200 kHz) excitation at a range of pulse fluences corresponding to the quoted photoexcitation densities. Solid lines are fits to the data using the model described by Stranks *et al.* (ref 27), allowing extraction of the quoted trap densities N_T.

on the surface of the perovskite material, with pyridine being more effective, reaching a "plateau" in PLQE at much lower excitation powers. We speculate that the reason for this could be that pyridine binds more strongly to the perovskite surface than thiophene and thus more successfully reduces the density of undercoordinated ions. It is interesting to note that even though the pyridine treatment results in a higher PLQE at low excitation fluences, we observe a marginally shorter PL lifetime compared to the thiophene-treated films. Although this appears to be inconsistent, it may imply that the treatments impact the radiative decay rate as well as the nonradiative decay rate, with the pyridine treatment speeding up the prior. Further work is required, however, in order to understand this peculiarity. We note that *tert*-butylpyridine (tBP) is often employed as an additive to the spiro-MeOTAD hole transporter. However, we have measured the impact of precoating the perovskite films with tBP, and we do not observe retardation in photoluminescence decay (see Supporting Information Figure S2). This may imply that the efficacy of the Lewis base treatment is strongly influenced by steric or inductive effects.

We have recently proposed a model to describe the evolution of photoexcited species (free charges and excitons) and the subsequent photoluminescence kinetics in these materials in the presence of N_T subgap electronic trap states.[27] Under photoexcitation, n_T traps are filled with electrons, which will result in a population of n_T photodoped holes in the valence band.[27] The total number of photogenerated holes at any point in time will be $n_h = n_e + n_T$, where n_e is the number of free electrons. The total concentration of photogenerated carriers (excluding trapped electrons and their corresponding holes) can then be defined $N = n_e + n_x$, where n_x is the concentration excitons. We can write rate equations for the evolution of these species and solve analytically to obtain an expression to describe the PL kinetics which can be fitted to the experimental data to determine the trap density N_T. Full details of the model are given in Stranks *et al.*[27] The key assumption is that the trapped electron is comparatively long-lived, which means the concentration of trapped electrons is constant over a PL decay measurement.

The intensity-dependent PL decays for both untreated and treated samples are shown in Figure 2.

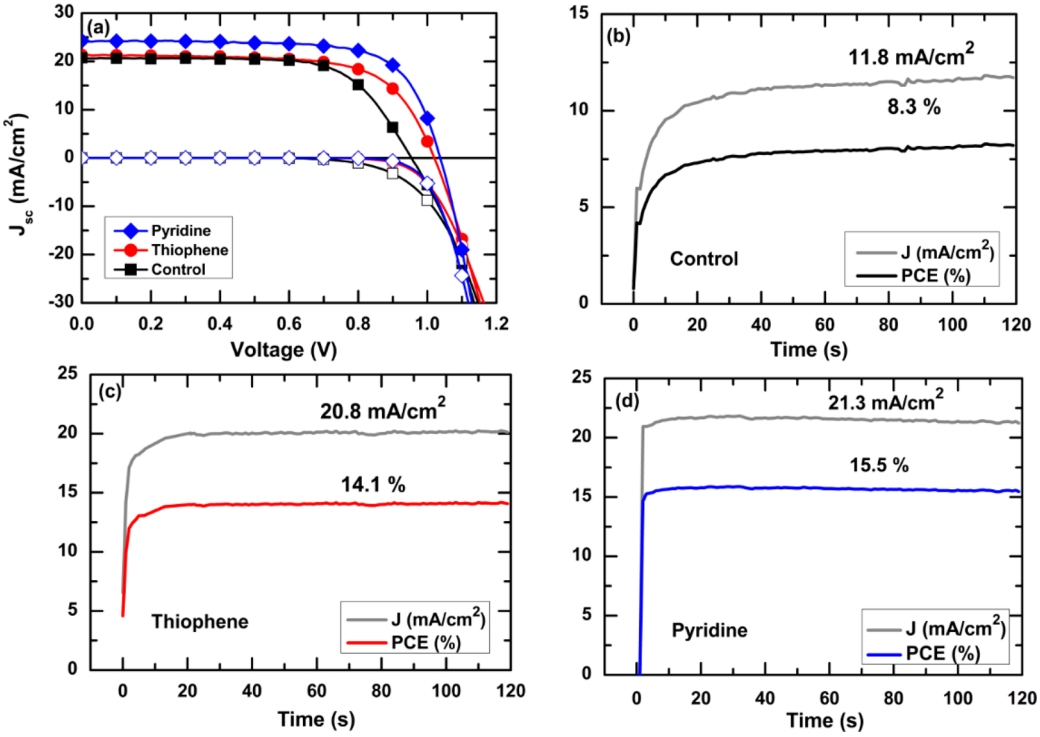

Figure 3. (a) Current−voltage (*J*−*V*) characteristics for the best control (black squares) and the thiophene-passivated (red circles) and pyridine-passivated (blue diamonds) devices. The power conversion efficiency of the control device is 13.1%, and the passivated devices are 15.3% (thiophene) and 16.5% (pyridine) under full sun illumination. Dark *J*−*V* curves are illustrated with hollow symbols. (b) Stabilized efficiency of control, (c) thiophene-, and (d) pyridine-passivated devices, measured by holding the device at its maximum power point for 120 s.

At low fluences, such as initial photoexcitation densities of $\sim 10^{15}$ cm^{-3}, recombination is dominated by near-monomolecular recombination between the dominant number of photodoped holes and the minority photoexcited electrons. At high fluences ($\sim 10^{17}$ cm^{-3}), traps are predominantly filled and the number of photoexcited electrons dominates over the photodoped holes, leading to a radiative bimolecular decay until low enough density is reached (at longer times) that the decay once more becomes monomolecular. The bimolecular decay rate will depend strongly upon the concentration of (untrapped) photogenerated carriers *N*, which in turn will be influenced by the density of available trap sites.

We have globally fitted the intensity-dependent PL decays with the model and determined the trap density of the as-prepared film to be 3.5×10^{16} cm^{-3}. For the thiophene-passivated film, this trap density is decreased 3-fold to 1.0×10^{16} cm^{-3}, while for the pyridine-passivated film, the extracted trap density is decreased by an order of magnitude, resulting in an inferred trap density of 0.2×10^{16} cm^{-3}. This is hence consistent with both the thiophene and pyridine treatments effectively passivating electronic trap sites in the organic−inorganic lead halide perovskites. We note, however, that this is quite a basic model with four main fitting parameters. While all of these parameters can be varied individually to obtain much closer fits than those shown in Figure 2, in this case, for simplicity, all other parameters were fixed, allowing only the trap density to vary. While this has resulted in slightly poorer fits for the highest excitation densities, we must note that this does not affect the calculation of the trap density of the films.

Having shown spectroscopic data which are consistent with thiophene and pyridine molecules passivating nonradiative decay sites in the perovskite absorber, here we present solution-processed planar heterojunction solar cells, fabricated according to literature.[29] The mixed-halide perovskite precursor solution (40 wt % 3:1 $CH_3NH_3I/PbCl_2$ in DMF) was spin-coated onto fluorine-doped tin oxide (FTO) substrates coated with a compact layer of TiO_2 and annealed under a nitrogen atmosphere (see Supporting Information for full experimental detail). The Lewis base treatments were then spin-coated onto the fully crystallized perovskite-coated substrates before the deposition of the HTM. The devices were completed with Au cathodes.

We show the current−voltage characteristics of the best devices in Figure 3. Both the thiophene and the pyridine treatments significantly increase the efficiency of the best planar heterojunction solar cells, and we observed an increase in the maximum power conversion efficiency from 13.1 to 15.3% with thiophene passivation and to 16.5% with pyridine passivation. Even more encouraging is the increase in average

performance and reduction in standard deviation, as we show in Table 1 and Supporting Information Figure S4. These results represent one of the highest reported efficiencies for planar heterojunction perovskite solar cells fabricated using a single-step solution deposition method. We show the solar cell performance parameters in Table 1.

It is frequently observed that perovskite solar cells exhibit hysteresis in the current−voltage curves; however, little is known about the source of this phenomenon.[30,31] We have recently shown that even though hysteresis is present in these devices, it is possible to achieve both stabilized current and efficiency from the meso-superstructured solar cell, which is close to that of the best scan. Interestingly, in the case of the planar heterojunction devices incorporating planar TiO_2 and spiro-OMeTAD n- and p-type charge collection layers, the stabilized power output is typically around one-half of what can be achieved *via* a fast scan.[31] In Figure 4b−d, we show the stabilized power output of the best devices from this study by holding them at their maximum power point voltage under simulated AM 1.5 100 mW cm^{-2} irradiance and measuring the photocurrent for 2 min. Encouragingly, with respect to the control devices, the stabilized power output is much improved with the pyridine and thiophene treatments, resulting in a stabilized power conversion efficiency for the planar heterojunction solar cells which closely approaches that of the fast scan. For the untreated device, the fast scan produces an efficiency of 13.1%, which then stabilizes at 8.3%, whereas for the thiophene-treated device, the fast scan produces an efficiency of 15.3%, which stabilizes at 14.1%, and for the pyridine-treated device, a scanned efficiency of 16.5% is produced with a stabilized output of 15.5%. If we define the photocurrent rise time to be the time taken to reach 95% of the maximum stabilized power output, the rise time reduces from 40 to 12 to less than 2 s (sampling time) for the control and the thiophene- and pyridine-treated devices, respectively. This is consistent with the theory that the hysteresis is influenced by the requirement for trap-filling and an increased ability to rapidly fill all the defect sites in the passivated films due to the lower trap density.

Annealing in selenium or sulfur atmosphere is a well-known passivation technique for thin film solar cells such as copper indium gallium selenide and copper zinc tin sulfide.[32−34] The sulfurization step typically takes place postannealing and serves to facilitate grain growth as well as to passivate surface states created during annealing due to sulfur losses.[34] In the case of these thin films, the loss of sulfur during the annealing process would cause unsaturated or

TABLE 1. Performance Parameters of Best Control and Passivated Devices[a]

	J_{sc} (mA/cm^2)	V_{oc} (V)	η (%)	η_{avg} (%)	FF (au)	η_{MPP} (%)	J_{MPP} (mA/cm^2)	η_{MPP}/η
control	20.7	0.95	13.1	12.1	0.68	8.3	11.8	0.63
thiophene	21.3	1.02	15.3	14.3	0.68	14.1	20.8	0.92
pyridine	24.1	1.05	16.5	15.5	0.72	15.5	21.3	0.94

[a] Device performance parameters for the champion devices of each variable, along with the stabilized efficiency and current values.

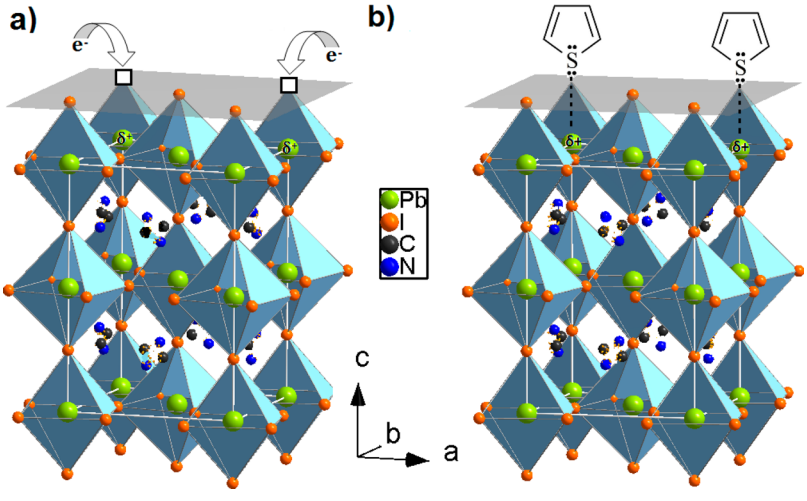

Figure 4. Possible nature of trap sites and proposed passivation mechanism. (a) Loss of iodine at the surface of the perovskite leads to vacancy sites (hollow boxes) and a resulting net positive charge residing on the Pb atom (shown in green). Photogenerated electrons are then able to fall into this Coulomb trap site, thus neutralizing the charge and rendering the crystal more stable. (b) Thiophene or pyridine molecules can donate electron density to the Pb and form a coordinate or dative covalent bond, effectively neutralizing the excess positive charge in the crystal.

under-coordinated metal ions most frequently found on the surface and at the grain boundaries of crystals. We propose that a similar effect takes place upon annealing the perovskite. During the annealing process of $MAPbX_3$ perovskites, halide and methylammonium ions can be lost from the crystal, resulting in under-coordinated Pb atoms both on the crystal surface and at the grain boundaries. Recent modeling and experimental studies have shown that these under-coordinated Pb atoms, and clusters in some cases, can act as electronic trap states within the perovskite material.[18,22] This under-coordination of the Pb atom could result in the formation of a net positive charge on the atom, which would then create favorable conditions for coordination, or bond formation with electron-rich molecules such as thiophene or other sufficiently weak Lewis bases. In the case of thiophene, and any such material which has a lone pair available for coordination, the electrostatic attraction between the positive charge on the metal and the lone pair could facilitate the formation of a coordinate or dative covalent bond. This positive charge can then be delocalized within a thiophene or pyridine molecule. This process is illustrated schematically in Figure 4. We must note, however, that this is only a postulation at this stage, and further studies are required to fully clarify the mechanism for the Lewis base treatments.

CONCLUSIONS

In summary, we have demonstrated that treatment of organic–inorganic metal halide perovskite films with the Lewis bases thiophene and pyridine can result in a significant decrease in the rate of nonradiative recombination in perovskite films. In so doing, we have increased the efficiency of solution-processed planar heterojunction perovskite solar cells from 13% to 15.3% and 16.5% using thiophene and pyridine treatments, respectively, and even more significantly achieved high stabilized power output. We have postulated that the Lewis base molecules bind to the under-coordinated Pb ions in the perovskite crystal, thus passivating these defect sites. Beyond use in solar cells, this passivation technique is likely to prove useful for many other perovskite-based optoelectronic applications such as lasers and light-emitting diodes.

MATERIALS AND METHODS

Fabrication of Planar Heterojunction Solar Cells. Planar heterojunction solar cells were fabricated utilizing previously published methods.[9,27] Concisely, FTO-coated glass sheets (7 Ωcm^{-1} Pilkington) were etched with zinc powder and HCl (3 M) to obtain the required electrode pattern. The sheets were then washed with soap (2% Hellmanex in water), deionized water, acetone, and methanol and finally treated under oxygen plasma for 10 min to remove the last traces of organic residues. A 100 nm thick compact layer of TiO_2 was then deposited on the glass using titanium isopropoxide diluted in anhydrous ethanol and sintered for 45 min at 500 °C. The 40 wt % perovskite precursor solution was then spin-coated directly onto the substrate in a nitrogen-filled glovebox. The substrate was then left to dry under N_2 for 30 min before being placed on a hot plate at 90 °C where it was annealed for 180 min. After being annealed, the substrate was allowed to cool to room temperature and neat thiophene (or pyridine diluted 1:10 vol/vol in chlorobenzene) was spin-coated on top of the perovskite layer, followed by the HTM. The HTM used in these experiments was an 8.5 wt % solution of spiro-OMeTAD (30 mol % of Li-TFSI and 80 mol % of tBP as additives) and was spin-coated onto the perovskite substrates at 2000 rpm. Then, 50 nm thick gold electrodes were deposited under high vacuum (10−6) through a shadow mask.

Fabrication of Spectroscopy Samples. Spectroscopy samples were fabricated on cleaned, plasma-etched glass, where the 40 wt % perovskite precursor solution was spin-coated onto the glass directly after plasma etching. As with the devices, this was done under inert atmosphere. Subsequent to the deposition of the perovskite layer, the substrates were left to dry for 30 min before being annealed for 180 min at 90 °C. The films were then coated with thiophene or pyridine as above before being coated with a 1% solution of poly(methyl methacrylate). Devices were typically stored in a desiccator in the dark for 12 h before spectroscopic investigation.

Solar Cell Characterization. Solar cell performance was measured using a class AAB ABET sun 2000 solar simulator that was calibrated to give simulated AM 1.5 sunlight at an irradiance of 100 mW/cm^2. The mismatch factor was estimated to be approximately 1.02 and applied when setting the intensity of the solar simulator. The irradiance was calibrated using an NREL-calibrated KG5-filtered silicon reference cell. Current–voltage curves were recorded using a sourcemeter (Keithley 2400, USA). All solar cells were masked with a metal aperture that was used to define the active area of the devices, which in this case was 0.0625 cm^2. All devices like the spectroscopy samples were stored in a desiccator in the dark for 12 h prior to testing.

Spectroscopy. Steady-state absorption spectra were acquired with a Varian Cary 300 UV/vis spectrophotometer. Steady-state photoluminescence quantum efficiency values were determined using a 532 nm CW laser excitation source (Suwtech LDC-800) to illuminate a sample in an integrating sphere (Oriel Instruments 70682NS) and the laser scatter and PL collected using a fiber-coupled detector (Ocean Optics MayaPro). The spectral response of the fiber-coupled detector setup was calibrated using a spectral irradiance standard (Oriel Instruments 63358). PLQE calculations were carried out using established techniques.[35] Time-resolved PL decays were acquired using a time-correlated single photon counting setup (FluoTime 300, PicoQuant GmbH). Samples were photoexcited using a 507 nm laser head (LDH-P-C-510, PicoQuant GmbH) with a pulse duration of 117 ps, fluences of ~0.03–3 $\mu J/cm^2$/pulse, and a repetition rate of 300 kHz.

Conflict of Interest: The authors declare no competing financial interest.

Acknowledgment. The research leading to these results has received funding from the European Union Seventh Framework Programme [FP7/2007-2013] under Grant Agreement No. 604032 of the MESO project. N.N. thanks the Government of the Republic of Trinidad and Tobago for additional financial support. S.D.S. would like to thank Worcester College, Oxford, for additional financial support. V.B. acknowledges the support of an Oxford Martin School Fellowship. The authors would also like to thank Dr. Amir Abbas Haghighirad, Dr. Sandeep K. Pathak, Tomas Leijtens, and Aditya Sadhanala for helpful discussions.

Supporting Information Available: Additional PL data, device statistics, and UV–vis data are given in the Supporting Information. This material is available free of charge *via* the Internet at http://pubs.acs.org.

REFERENCES AND NOTES

1. Kojima, A.; Teshima, K.; Shirai, Y.; Miyasaka, T. Organometal Halide Perovskites as Visible-Light Sensitizers for Photovoltaic Cells. *J. Am. Chem. Soc.* **2009**, *131*, 6050–6051.
2. Im, J.-H.; Lee, C.-R.; Lee, J.-W.; Park, S.-W.; Park, N.-G. 6.5% Efficient Perovskite Quantum-Dot-Sensitized Solar Cell. *Nanoscale* **2011**, *3*, 4088–4093.
3. Kim, H.-S.; Lee, C.-R.; Im, J.-H.; Lee, K.-B.; Moehl, T.; Marchioro, A.; Moon, S.-J.; Humphry-Baker, R.; Yum, J.-H.; Moser, J. E.; *et al.* Lead Iodide Perovskite Sensitized All-Solid-State Submicron Thin Film Mesoscopic Solar Cell with Efficiency Exceeding 9%. *Sci. Rep.* **2012**, 2.
4. Lee, M. M.; Teuscher, J.; Miyasaka, T.; Murakami, T. N.; Snaith, H. J. Efficient Hybrid Solar Cells Based on Meso-Superstructured Organometal Halide Perovskites. *Science* **2012**, *338*, 643–647.
5. Chang, J. A.; Im, S. H.; Lee, Y. H.; Kim, H.-j.; Lim, C.-S.; Heo, J. H.; Seok, S. I. Panchromatic Photon-Harvesting by Hole-Conducting Materials in Inorganic–Organic Heterojunction Sensitized-Solar Cell through the Formation of Nanostructured Electron Channels. *Nano Lett.* **2012**, *12*, 1863–1867.
6. You, J.; Hong, Z.; Yang, Y.; Chen, Q.; Cai, M.; Song, T.-B.; Chen, C.-C.; Lu, S.; Liu, Y.; Zhou, H.; *et al.* Low-Temperature Solution-Processed Perovskite Solar Cells with High Efficiency and Flexibility. *ACS Nano* **2014**, *8*, 1674–1680.
7. Ball, J. M.; Lee, M. M.; Hey, A.; Snaith, H. Low-Temperature Processed Mesosuperstructured to Thin-Film Perovskite Solar Cells. *Energy Environ. Sci.* **2013**, *6*, 1739–1743.
8. Bi, D.; Moon, S.-J.; Haggman, L.; Boschloo, G.; Yang, L.; Johansson, E. M. J.; Nazeeruddin, M. K.; Gratzel, M.; Hagfeldt, A. Using a Two-Step Deposition Technique To Prepare Perovskite ($CH_3NH_3PbI_3$) for Thin Film Solar Cells Based on ZrO_2 and TiO_2 Mesostructures. *RSC Adv.* **2013**, *3*, 18762–18766.
9. Eperon, G. E.; Burlakov, V. M.; Docampo, P.; Goriely, A.; Snaith, H. J. Morphological Control for High Performance, Solution-Processed Planar Heterojunction Perovskite Solar Cells. *Adv. Funct. Mater.* **2014**, *24*, 151–157.
10. Eperon, G. E.; Stranks, S. D.; Menelaou, C.; Johnston, M. B.; Herz, L. M.; Snaith, H. J. Formamidinium Lead Trihalide: A Broadly Tunable Perovskite for Efficient Planar Heterojunction Solar Cells. *Energy Environ. Sci.* **2014**, *7*, 982–988.
11. Liu, D.; Kelly, T. L. Perovskite Solar Cells with a Planar Heterojunction Structure Prepared Using Room-Temperature Solution Processing Techniques. *Nat. Photonics* **2014**, *8*, 133–138.
12. Liu, M.; Johnston, M. B.; Snaith, H. J. Efficient Planar Heterojunction Perovskite Solar Cells by Vapour Deposition. *Nature* **2013**, *501*, 395–398.
13. Docampo, P.; Ball, J. M.; Darwich, M.; Eperon, G. E.; Snaith, H. J. Efficient Organometal Trihalide Perovskite Planar-Heterojunction Solar Cells on Flexible Polymer Substrates. *Nat. Commun.* **2013**, 4.
14. Jeng, J.-Y.; Chiang, Y.-F.; Lee, M.-H.; Peng, S.-R.; Guo, T.-F.; Chen, P.; Wen, T.-C. $CH_3NH_3PbI_3$ Perovskite/Fullerene Planar-Heterojunction Hybrid Solar Cells. *Adv. Mater.* **2013**, *25*, 3727–3732.
15. Wang, Q.; Dong, Q.; Xiao, Z.; Yuan, Y.; Huang, J. Large Fill-Factor Bilayer Iodine Perovskite Solar Cells Fabricated by Low-Temperature Solution-Process. *Energy Environ. Sci.* **2014**, *7*, 2359–2365.
16. Malinkiewicz, O.; Yella, A.; Lee, Y. H.; Espallargas, G. M.; Graetzel, M.; Nazeeruddin, M. K.; Bolink, H. J. Perovskite Solar Cells Employing Organic Charge-Transport Layers. *Nat. Photonics* **2014**, *8*, 128–132.
17. Skromme, B. J.; Sandroff, C. J.; Yablonovitch, E.; Gmitter, T. Effects of Passivating Ionic Films on the Photoluminescence Properties of GaAs. *Appl. Phys. Lett.* **1987**, *51*, 2022–2024.
18. Yin, W.-J.; Shi, T.; Yan, Y. Unusual Defect Physics in $CH_3NH_3PbI_3$ Perovskite Solar Cell Absorber. *Appl. Phys. Lett.* **2014**, *104*, 063903.
19. Kim, J.; Lee, S.-H.; Lee, J. H.; Hong, K.-H. The Role of Intrinsic Defects in Methylammonium Lead Iodide Perovskite. *J. Phys. Chem. Lett.* **2014**, *5*, 1312–1317.
20. Deschler, F.; Price, M.; Pathak, S.; Klintberg, L. E.; Jarausch, D.-D.; Higler, R.; Hüttner, S.; Leijtens, T.; Stranks, S. D.; Snaith, H. J.; *et al.* High Photoluminescence Efficiency and Optically Pumped Lasing in Solution-Processed Mixed Halide Perovskite Semiconductors. *J. Phys. Chem. Lett.* **2014**, *5*, 1421–1426.
21. Leijtens, T.; Stranks, S. D.; Eperon, G. E.; Lindblad, R.; Johansson, E. M. J.; McPherson, I. J.; Rensmo, H.; Ball, J. M.; Lee, M. M.; Snaith, H. J. Electronic Properties of Meso-Superstructured and Planar Organometal Halide Perovskite Films: Charge Trapping, Photodoping, and Carrier Mobility. *ACS Nano* **2014**, *8*, 7147–7155.
22. Shkrob, I. A.; Marin, T. W. Charge Trapping in Photovoltaically Active Perovskites and Related Halogenoplumbate Compounds. *J. Phys. Chem. Lett.* **2014**, *5*, 1066–1071.
23. Abate, A.; Saliba, M.; Hollman, D. J.; Stranks, S. D.; Wojciechowski, K.; Avolio, R.; Grancini, G.; Petrozza, A.; Snaith, H. J. Supramolecular Halogen Bond Passivation of Organic–Inorganic Halide Perovskite Solar Cells. *Nano Lett.* **2014**, *14*, 3247–3254.
24. Itzhaik, Y.; Niitsoo, O.; Page, M.; Hodes, G. Sb_2S_3-Sensitized Nanoporous TiO_2 Solar Cells. *J. Phys. Chem. C* **2009**, *113*, 4254–4256.
25. Roe, A. L.; Hayes, K. F.; Chisholm-Brause, C.; Brown, G. E.; Parks, G. A.; Hodgson, K. O.; Leckie, J. O. *In Situ* X-ray Absorption Study of Lead Ion Surface Complexes at the Goethite–Water Interface. *Langmuir* **1991**, *7*, 367–373.
26. Fox, M. *Optical Properties of Solids*; Oxford University Press: Oxford, 2010.
27. Stranks, S. D.; Burlakov, V. M.; Leijtens, T.; Ball, J. M.; Goriely, A.; Snaith, H. J. Recombination Kinetics in Organic-Inorganic Perovskites: Excitons, Free Charge and Sub-Gap States. *Phys. Rev. Applied* **2014**, in press.
28. Stranks, S. D.; Eperon, G. E.; Grancini, G.; Menelaou, C.; Alcocer, M. J. P.; Leijtens, T.; Herz, L. M.; Petrozza, A.; Snaith, H. J. Electron–Hole Diffusion Lengths Exceeding 1 Micrometer in an Organometal Trihalide Perovskite Absorber. *Science* **2013**, *342*, 341–344.
29. Eperon, G. E.; Burlakov, V. M.; Docampo, P.; Goriely, A.; Snaith, H. J. Morphological Control for High Performance, Solution-Processed Planar Heterojunction Perovskite Solar Cells. *Adv. Funct. Mater.* **2014**, *24*, 151–157.
30. Dualeh, A.; Moehl, T.; Tétreault, N.; Teuscher, J.; Gao, P.; Nazeeruddin, M. K.; Grätzel, M. Impedance Spectroscopic Analysis of Lead Iodide Perovskite-Sensitized Solid-State Solar Cells. *ACS Nano* **2014**, *8*, 362–373.
31. Snaith, H. J.; Abate, A.; Ball, J. M.; Eperon, G. E.; Leijtens, T.; Noel, N. K.; Stranks, S. D.; Wang, J. T.-W.; Wojciechowski, K.; Zhang, W. Anomalous Hysteresis in Perovskite Solar Cells. *J. Phys. Chem. Lett.* **2014**, *5*, 1511–1515.
32. Mitzi, D. B.; Gunawan, O.; Todorov, T. K.; Wang, K.; Guha, S. The Path towards a High-Performance Solution-Processed Kesterite Solar Cell. *Sol. Energy Mater. Sol. Cells* **2011**, *95*, 1421–1436.
33. Hlaing Oo, W. M.; Johnson, J. L.; Bhatia, A.; Lund, E. A.; Nowell, M. M.; Scarpulla, M. A. Grain Size and Texture of Cu_2ZnSnS_4 Thin Films Synthesized by Cosputtering Binary Sulfides and Annealing: Effects of Processing Conditions and Sodium. *J. Electron. Mater.* **2011**, *40*, 2214–2221.
34. Khalkar, A.; Lim, K.-S.; Yu, S.-M.; Patole, S. P.; Yoo, J.-B. Effect of Growth Parameters and Annealing Atmosphere on the Properties of Cu_2ZnSnS_4 Thin Films Deposited by Cosputtering. *Int. J. Photoenergy* **2013**, *2013*, 7.
35. de Mello, J. C.; Wittmann, H. F.; Friend, R. H. An Improved Experimental Determination of External Photoluminescence Quantum Efficiency. *Adv. Mater.* **1997**, *9*, 230–232.